ACS APPLIED MATERIALS & INTERFACES

RESEARCH ARTICLE

www.acsami.org

Adsorption of Nonlamellar Nanostructured Liquid-Crystalline Particles to Biorelevant Surfaces for Improved Delivery of Bioactive Compounds

Yao-Da Dong,[†] Ian Larson,[†] Timothy J. Barnes,[‡] Clive A. Prestidge,[‡] and Ben J. Boyd*[,†]

[†]Drug Delivery, Disposition and Dynamics, Monash Institute of Pharmaceutical Sciences, Monash University (Parkville Campus), 381 Royal Pde, Parkville, Victoria, Australia

[‡]Ian Wark Research Institute, University of South Australia, Mawson Lakes Boulevard, Mawson Lakes, South Australia, Australia

ABSTRACT: The adsorption of nanostructured lyotropic liquid-crystal particles, cubosomes and hexosomes, at surfaces was investigated for potential use in surface-specific agrochemical delivery. Adsorption of phytantriol (PHYT) and glyceryl monooleate (GMO)-based cubosomes and hexosomes, stabilized using Pluronic F127, at tristearin-coated (model leaf surface) and uncoated zinc selenide surfaces was studied using attenuated total reflectance Fourier transform IR (ATR-FTIR) spectroscopy, by quantifying the IR absorbance due to the lipid components of the particles over time. The delivery of an encapsulated hydrophobic model herbicide [dichlorodiphenyldichloroethylene (DDE)] was also examined on the model and real leaf surfaces. The adsorption behavior of the particles by ATR-FTIR was dependent on the internal nanostructure and lipid composition, with PHYT cubosomes adsorbing more avidly at tristearin surfaces than GMO-based cubosomes or hexosomes. There was a direct correlation between DDE associated with the surfaces and the particle adsorption observed in the ATR-FTIR study, strongly implicating particle adsorption with the delivery efficiency. Differences between the mode of interaction of the Pluronic stabilizer with the different lipids and particle nanostructures were proposed to lead to differences in the particle adsorption behavior.

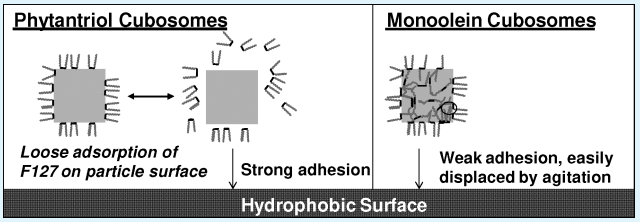

KEYWORDS: liquid crystal, cubosomes, hexosomes, surface adsorption, interfacial properties

INTRODUCTION

A growing number of amphiphilic molecules are being discovered that form nanostructured nonlamellar phases such as the inverse bicontinuous cubic (V_2) and inverse hexagonal (H_2) lyotropic liquid crystals (LCs) in excess water.[1−4] These materials are considered to have great potential in the field of drug encapsulation and delivery[5−7] because they can provide a persistent drug reservoir and sustained release for molecules with widely varying polarity.[8,9] Glyceryl monooleate (GMO)[10−17] and phytantriol (PHYT)[18,19] are two lipids with such properties that have received much recent interest. Both molecules form a bicontinuous cubic phase at ambient temperature in excess water. The addition of small amounts (5% w/w) of vitamin E acetate (VitEA) to PHYT induces the formation of an inverse hexagonal phase at ambient temperature in excess water, providing the opportunity to study the different phase structures with only a subtle change to the overall chemical composition.[19]

These materials may be dispersed to form submicrometer particles, termed "cubosomes" and "hexosomes", that retain the internal structure of the nondispersed cubic and hexagonal phases, respectively (Figure 1).[20−22] The particles are not colloidally stable and are typically dispersed with the addition of a stabilizer, most often the block copolymer Pluronic F127 (F127). Topical application of bulk and dispersed inverse cubic phases prepared from PHYT and GMO to the skin has demonstrated enhanced active penetration and prolonged activity.[23−27]

The enhanced delivery of actives to the skin using dispersed LC systems[23,26,28−32] suggests the possibility that the particle may enhance the delivery of active molecules to other biorelevant hydrophobic surfaces, such as plant leaf surfaces. To date, interaction of the LC particles with such surfaces has not been studied. In fact, studies on the adsorption behavior of LC particles are limited and difficult to compare because of variations in the stabilizer and lipid compositions used in such studies.[33−37] As such, systematic studies on the particle adsorption behavior at biorelevant surfaces are still required to better understand the surface properties of nanostructured LC particles. In particular, the potential to produce particles with differing internal phase structures through subtle changes in the composition leads to the hypothesis that the internal structure will impact the external surface structure of the particles, which, in turn, is expected to influence the adsorption behavior.

The use of the stabilizer F127 to stabilize GMO-based cubosomes is known to transform the internal phase structure from the $V_{2(Pn3m)}$ structure to the $V_{2(Im3m)}$ phase. No such change occurs for PHYT-based cubosomes.[19] This indicates a different mode of interaction between F127 and GMO compared to that between F127 and PHYT, which is also anticipated to play a role in the interfacial behavior of cubosomes. Hence, the choice

Received: March 11, 2011
Accepted: April 21, 2011
Published: April 21, 2011

dx.doi.org/10.1021/am2003069 | *ACS Appl. Mater. Interfaces* 2011, 3, 1771–1780

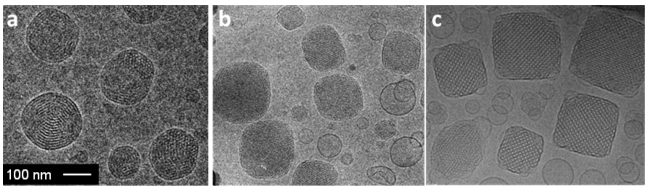

Figure 1. Cryo-TEM images of PHYT + 10% VitEA (w/w) hexosomes (A), PHYT cubosomes (B), and GMO cubosomes (C). Both GMO and PHYT cubosome systems show the presence of vesicles, which are absent in the hexosome system.

of lipid to prepare the particles may also be an important determinant in the interfacial adsorption behavior.

Therefore, in this study, the interfacial adsorption of cubosomes and hexosomes was investigated in the context of determining their potential as foliar-targeted agrochemical delivery agents. The effect of changes of the particle internal structure on the surface adsorption and retention was examined using attenuated total reflectance Fourier transform IR (ATR-FTIR) spectroscopy. In addition, the correlation between the particle adsorption and surface localization of an encapsulated model agrochemical compound, dichlorodiphenyldichloroethylene (DDE), was examined by quantifying the amount of active delivered to model and real leaf surfaces.

EXPERIMENTAL SECTION

Materials. Phytantriol (PHYT) was purchased from Roche (Grenzach-Wyhlen, Germany) with a nominal purity of >96.6%. Vitamin E acetate (VitEA) was purchased from Sigma Aldrich Chemie (Steinhiem, Germany) with a nominal purity of ≥96%. Myverol 18-99K was donated by Kerry Bio-Science (Norwich, NY) and was used for the preparation of glyceryl monooleate (GMO)-based samples. The analytical data indicate that Myverol 18-99K (certificate no. 31500455) contains 58.3% GMO (C18:1), 12.2% glyceryl monolinoleate (C18:2), 5.1% glyceryl monolinolenate (C18:3), 3.9% glyceryl monopalmitate (C16:0), 1.7% glyceryl monostearate (C18:0), 0.96% glyceryl monogadoleate (C20:1), 0.2% glyceryl arachidonate (C20:4), 0.1% free fatty acids, and 0.4% glycerol. Trace amounts of unquantified diglycerides are also believed to be present. Pluronic F-127 (analytical grade) was purchased from BASF (Somerset, NJ).

Soluene-350 tissue solubilizer and Starscint liquid scintillation cocktail were purchased from Packard Bioscience (Meriden, CT). ^{14}C-dichlorodiphenyldichloroethylene (DDE) was purchased from American Radiolabeled Chemicals (St Louis, MO). Glyceryl tristearate (tristearin) was purchased from Sigma Aldrich (St. Louis, MO). Milli-Q-grade water (resistivity > 18.2 MΩ cm^{-1} at 25 °C) purified through a Millipore system (Sydney, Australia) was used for the preparation of aqueous systems.

Sample Preparation. The preparation process for the dispersed LC systems was reported previously.[19] Briefly, 1.0 g of lipid was weighed into a glass vial. A total of 9.0 g of water containing F127 (1% w/w) was added immediately prior to dispersion. Dispersion was achieved by ultrasonication (Misonix XL 2000, Misonix Inc., Farmingdale, NY) for 20 min in pulse mode (0.5 s pulses interrupted by 0.5 s breaks) at 40% of the maximum power, resulting in a milky dispersion. For systems consisting of a mixture of different lipids (e.g., PHYT and VitEA), the lipids were premixed using a roller mixer for at least 1 week prior to the phase sample preparation. For DDE-loaded dispersions, 20 μL of DDE with a nominal radioactivity of 0.1 mCi mL^{-1} (a specific activity of 10−30 mCi mmol^{-1}) in toluene was dried in a glass vial and combined with 1 g of lipids. The mixture was equilibrated by mixing on a roller mixer for 72 h and then sonicated after the addition of a F127 solution (1% w/w) to form LC dispersions. After ultrasonication, the samples were diluted to the required working concentration with water. All systems were stored at 25 °C for at least 2 days prior to further use to allow for equilibration of the components.

Table 1. Particle Sizes of the Cubosomes and Hexosomes Used in This Study[a]

lipid	internal phase[b]	size (nm)	polydispersity index
GMO	$V_{2(Im3m)}$	194.0 ± 0.2	0.15 ± 0.02
PHYT	$V_{2(Pn3m)}$	268.8 ± 0.9	0.18 ± 0.02
PHYT + 10% VitEA	H_2	251.6 ± 0.7	0.24 ± 0.02

[a] The lipid to Pluronic F127 ratio was 9:1 (w/w) in water at 25 °C (mean ± SD; n = 9). [b] Internal phase from small-angle X-ray scattering.[19]

The particle size distribution for dispersed LC systems is shown in Table 1. The particle size was approximately 200 nm for GMO-based cubosomes and approximately 250 nm for PHYT-based cubosomes and hexosomes, consistent with previous reports.[19] All systems showed comparable size distributions, with polydispersity indices ≤0.25 in water. The radioactivity of the dispersions was analyzed by liquid scintillation counting on a Packard Tri-Carb 2000CA liquid scintillation analyzer (Meriden, CT). The sizes of the dispersed particles were measured using a Zetasizer Nano ZS (Malvern Instruments, Worcestershire, U.K.).

Quantitation of Particle Adsorption at Surfaces by ATR-FTIR. The adsorption of cubosomes and hexosomes, based on PHYT and GMO, at hydrophilic [bare zinc selenide (ZnSe)] and hydrophobic (tristearin) surfaces was studied using ATR-FTIR spectroscopy in a manner similar to that previously reported for liposomes.[38]

Spectra were recorded with a Bio-Rad (Digilab) Excaliber FTS 3000 spectrophotometer in ATR mode. The trough sample cell had a ZnSe reflection element and a surface area of 5.0 × 10^{-4} m^2, with an angle of incidence of 45° at room temperature (25 °C).

Prior to the experiments, the ZnSe surface was cleaned with chloroform, ethanol, and water in that order. For adsorption on tristearin surfaces, a tristearin film (6.4 mg m^{-2}) was applied on the clean ZnSe surface by drying a chloroform-based solution.

LC dispersion (1.5 mL) was placed in the sample trough of the ATR cell, and IR spectra were recorded as a function of time for 100 min, with water background subtraction. After 100 min, the solution was manually agitated for 2 min by repeatedly drawing up and reapplying 0.5 mL of the dispersion solution in the sample cell using a pipet. The effects of agitation on adsorbed aggregates provided an indication of the strength of the adhesion to the surface.

LC particle adsorption was monitored from the absorbance of the C−H stretching vibrations attributed to the CH_3 (ν_{as} = 2953 cm^{-1}; ν_s = 2869 cm^{-1}) and CH_2 (ν_{as} = 2926 cm^{-1}; ν_s = 2853 cm^{-1}) moieties for PHYT and GMO, respectively (Figure 2).[39,40] Spectra were determined by coadding 32 scans at a resolution of 4.0 cm^{-1}; the detection limit was less than 0.005 absorbance units.

The mass of lipid adsorbed was determined from calibration curves, between 0 and 30 mg m^{-2}. Known masses of lipid and stabilizer in the appropriate proportion were applied to the surface as a chloroform solution. The solvent was evaporated to leave a known mass deposited on the crystal surface.

Retention of the Radiolabeled Active on Model Leaf Surfaces. Glass microscope slide coverslips (22 mm × 22 mm, Menzel-Glaser, Germany) were cleaned by repeated sonication in chloroform, ethanol and water and then dried at 60 °C in an oven. The hydrophobic tristearin layer (6.8 mg slide^{-1}, 14 g m^{-2}) was prepared by drying a tristearin solution in chloroform in an 80 °C oven for 30 min. The coverslips were then stored at 60 °C overnight. This

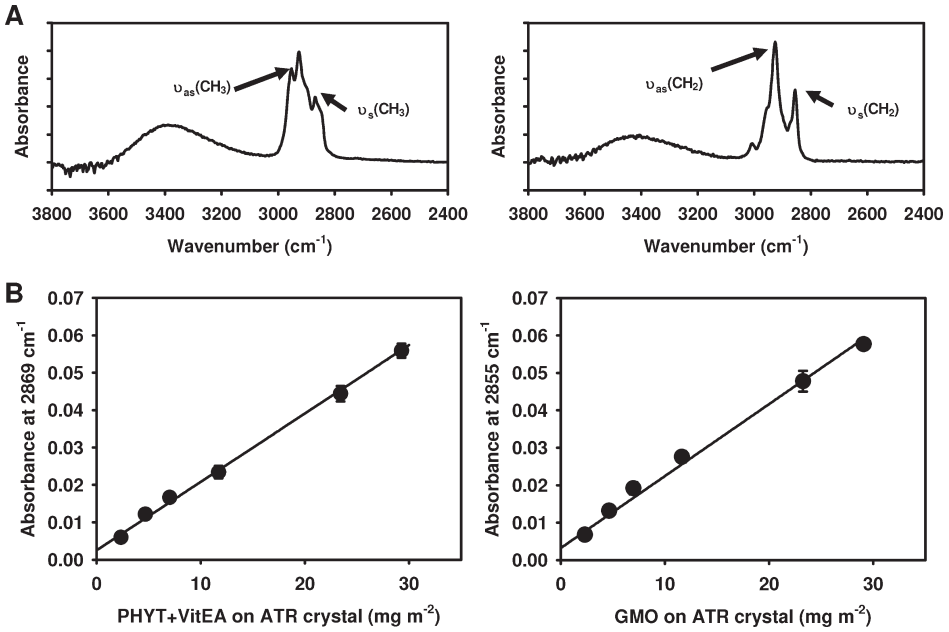

Figure 2. (A) IR spectra of deposited PHYT + VitEA (left) and GMO (right) with lipids and F127 at a weight ratio of 9:1, on the ZnSe crystal. (B) Calibration curve of IR absorbance at 2869 and 2855 cm^{-1} for the respective systems as a function of the amount of material deposited on the crystal (mean ± SD; $n = 6$). The assignments of vibration modes for PHYT was based on a Raman and FTIR spectroscopy study of the PHYT + water cubic phase (ν_a, symmetric stretching; ν_{as}, asymmetric stretching).[39]

procedure resulted in the formation of visually smooth opaque tristearin layers of visual uniform thickness on the coverslips.

The coverslips, either uncoated or coated (on the one side) with tristearin (TS-coated), were fully immersed vertically in DDE-loaded LC dispersions. The working concentration for the lipids in the cubosome and hexosome dispersion was 7.5 mg mL^{-1} to ensure that systems were at the plateau seen in adsorption isotherms obtained by ATR-FTIR. After immersion for 3 h, the glass slides were removed and rinsed by repeated immersion in beakers containing water (5 × 20 mL) to remove nonadsorbed materials from the surface. The residual adsorbed material, and tristearin for the TS-coated coverslips, was removed from the glass by immersing the slide in 3 mL of Soluene-350 for 2 h. The mixtures were vortex-mixed with 35 mL of Starscint, then transferred to 2 × 20 mL polypropylene scintillation vials, and analyzed for total radioactivity by liquid scintillation counting.

Leaves of *Hebe rakaiensis* (selected for uniform leaf dimensions) were freshly picked (<24 h before use) from a local garden (Melbourne, Australia) and selected for consistent size (approximately 20 mm × 10 mm) and weight (90 ± 4 mg). The leaves were rinsed thoroughly with water and blotted dry with low lint tissue (Kimwipes, Kimberly-Clark Professional, Milsons Point, Australia).

The leaf adsorption experiment was carried out as described for the tristearin model surface with DDE-loaded LC dispersions. After immersion of the leaves in a cubosome or hexosome dispersion for 3 h, the leaves were removed and rinsed by immersion in water (5 × 20 mL). The leaves were then completely digested through incubation overnight at 60 °C in 3 mL of Soluene-350, and the resulting liquid was subsequently bleached with 600 μL of 30% hydrogen peroxide for 3 h. The contents were then vortex-mixed with 70 mL of Starscint, transferred to 4 × 20 mL polypropylene scintillation vials, and analyzed for total radioactivity by liquid scintillation counting.

RESULTS

Calibration Curve for the Adsorption of Cubosomes and Hexosomes on the ATR-FTIR Crystal. The ATR-FTIR method allows quantitation of lipid on the surface by taking advantage of the unique absorbance "fingerprint" for the formulation lipids. For these experiments, it was assumed that lipid was deposited only in particle form and that the IR absorbance was due to the lipid molecules comprising the LC particles. The surface concentration of LC particles was ascertained by comparing the absorbance due to the C−H stretch against a calibration curve constructed for the particular lipid from which the particles were prepared.

Figure 2A shows typical IR spectra for the deposited PHYT + VitEA mixture and for GMO, with lipid and a F127 ratio of 9:1 (w/w). (PHYT alone gave a FTIR spectrum identical with that of PHYT + VitEA.) The resulting calibration curves (Figure 2B) illustrated a linear relationship between the absorbance and concentration in agreement with the Beer−Lambert law ($R^2 \geq 0.99$) and therefore enabled surface concentrations of lipid from LC particles to be determined from absorbance measurements. When the surface concentration was >5 mg m^{-2}, the assay validation yielded accuracy and precision at ±10%, and between 2 and <5 mg m^{-2}, the accuracy and precision were ±20%.

Adsorption of Cubosomes and Hexosomes onto Bare ZnSe and TS-Coated Surfaces. Figure 3 shows IR spectra for the ZnSe and tristearin surfaces after 100 min of exposure to a F127 solution or LC systems. The uppermost spectrum was obtained after 100 min of exposure of the ZnSe surface to a F127 solution. The spectrum showed no distinguishable peaks, indicating that it does not absorb in the region of interest and therefore its presence does not complicate the quantitation of PHYT or GMO adsorption. In comparison, the IR spectra upon exposure to hexosomes and cubosomes showed the same C−H absorbance spectra as those obtained for the cast lipid in the calibration spectra in Figure 2. This indicates the presence of cubosomes and hexosomes on both ZnSe and TS-coated surfaces. The broad minimum in the O−H stretch region

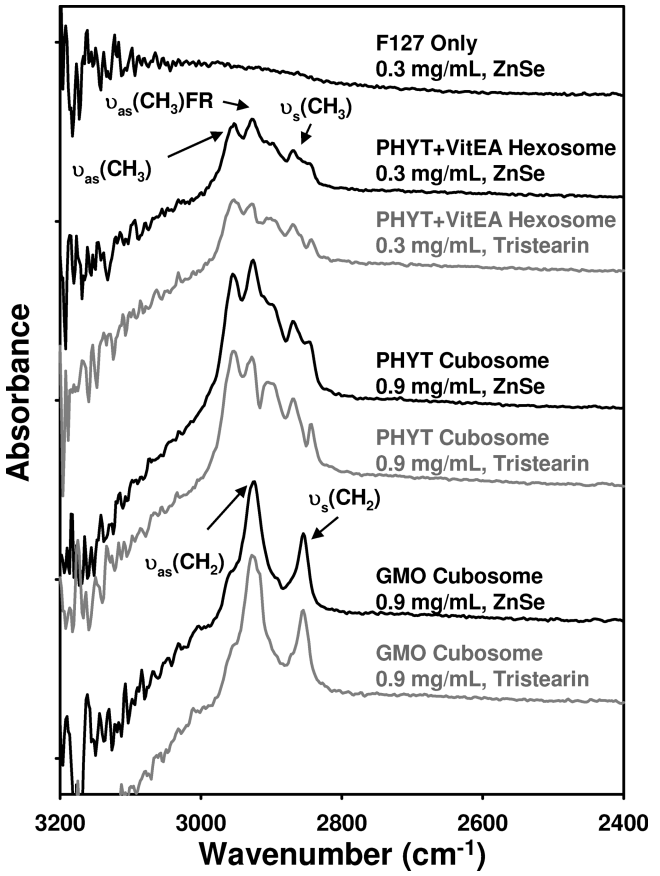

Figure 3. IR spectra of ZnSe and TS-coated surfaces after 100 min of exposure to different systems, highlighting (top) the lack of distinguishable peaks for the F127 solution and the differences in the position and relative intensity of the absorbance peaks on the different surfaces (ν_s, symmetric stretching; ν_{as}, asymmetric stretching; FR, Fermi resonance).[39,58]

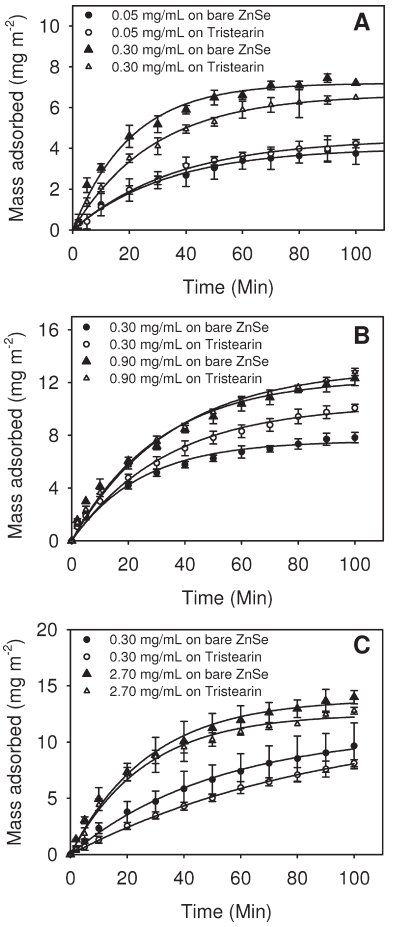

Figure 4. Adsorption of PHYT + VitEA hexosomes (A), PHYT cubosomes (B), and GMO cubosomes (C) on TS-coated and ZnSe surfaces as a function of time. For PHYT + VitEA hexosomes and PHYT cubosomes, the IR absorbance at 2869 cm^{-1} was used to quantify the mass adsorbed, while for GMO cubosomes, the absorbance at 2855 cm^{-1} was used (mean ± SD; $n = 3$). Solid lines indicate the best fit for each data set.

(3100−3400 cm^{-1}) of the background-subtracted FTIR spectra also supports the presence of LC particles on the surfaces because the reduced intensity at wavenumbers <3000 cm^{-1} indicates the displacement of water from the surface by lipid during particle adsorption. The penetration of the evanescent sensing wave in FTIR measurements beyond the surface of the crystal and into the sample is ∼1.66 μm;[41] if a single monolayer was deposited from the solution onto the surface, the decrease in the water content within the detection volume would be negligible.

The position of the symmetric and asymmetric stretching band maxima between 2965 and 2845 cm^{-1} provides qualitative information about the conformational order of lipids.[42] The diminished CH_3 stretch Fermi resonance maximum at 2926 cm^{-1} for the adsorption of hexosomes at the TS-coated surface compared to the ZnSe surface indicates that the conformational order of the adsorbed lipids was different on the two surfaces.

The IR spectra in Figure 3 for PHYT cubosomes were very similar to those of the PHYT + VitEA hexosomes. Specifically, the diminished CH_3 stretch Fermi resonance maximum at 2926 cm^{-1} for material adsorbed on the TS-coated surface compared to that on the ZnSe surface was apparent. This indicates that, like hexosomes, the conformational order of the adsorbed lipids was different on the two surfaces.

The IR spectra obtained during adsorption of GMO cubosomes also showed small upward shifts in the peak positions (∼2 cm^{-1} for the symmetric and asymmetric stretches of CH_2) for adsorption on TS-coated surfaces compared to ZnSe surfaces (Figure 3). Upward shifts in the peak positions of CH_2 stretches are usually associated with the introduction of conformational disorder in the alkyl chain,[43,44] again indicating that the conformational order of the adsorbed lipids was different on the two surfaces.

Kinetics of Adsorption. The particle adsorption at the TS-coated and ZnSe surfaces as a function of time are given in Figure 4. In general, the adsorption kinetics for all LC particle systems can be described by the first-order process

$$\Gamma(t) = \Gamma_\infty(1 - e^{-kt})$$

where k is the rate constant for particle adsorption and t is the time. The typical kinetic parameters, Γ_∞ and k, for adsorption are given in Table 2.

In all cases, the surface adsorption of cubosomes and hexosomes was at or very close to equilibrium after 100 min (Figure 4). Each type of particle showed an increased rate of adsorption and

Table 2. First-Order Kinetic Parameters for LC Particle Adsorption at the Bare ZnSe or TS-Coated Surface

particle	lipid (mM)	surface	Γ_∞ (mg m^{-2})	$k \times 10^{-2}$ (min^{-1})
PHYT + VitEA	0.9	ZnSe	7.2	4.8
hexosome	0.9	tristearin	6.6	3.5
	2.6	ZnSe	6.0	6.3
	2.6	tristearin	6.9	4.4
PHYT	0.9	ZnSe	7.4	3.8
cubosome	0.9	tristearin	10.2	3.0
	2.7	ZnSe	11.9	3.4
	2.7	tristearin	12.4	3.0
GMO	0.9	ZnSe	11.5	2.1
cubosome	0.9	tristearin	12.4	1.2
	2.6	ZnSe	13.9	3.3
	2.6	tristearin	13.9	2.3

increased equilibrium mass adsorbed with increased concentration. A greater adsorption rate at the more hydrophilic bare ZnSe crystal than at the TS-coated surface was also observed for all systems. There were, however, differences in the adsorption properties between particle species.

The hexosomes (Figure 4A) showed the highest rate of adsorption but the lowest mass adsorbed compare to cubosomes (Figure 4B) on both ZnSe and TS-coated surfaces. A higher rate of adsorption on the ZnSe surface was found compared to the TS-coated surface, but the type of surface had minimal bearing on the mass adsorbed at the plateau. In addition, at lower concentrations, PHYT cubosomes showed greater adsorbed mass at the plateau for the more hydrophobic TS-coated surface than the ZnSe surface. At the higher concentration ($\geq$0.9 mg mL^{-1}), however, a minimal difference in mass adsorbed at the plateau was observed for the two surfaces.

GMO cubosomes (Figure 4C) showed a lower rate of adsorption compared to the PHYT-based particles. The equilibrium mass adsorbed at higher concentrations for GMO cubosomes was similar to that for PHYT cubosomes, but there were minimal differences in mass adsorbed on the different surfaces, at both high and low concentrations. Because of the insensitivity of the FTIR method to F127 adsorption at surfaces (Figure 3), it was not possible to decouple F127 adsorption from that of the particles.

Adsorption Isotherms. Figure 5 compares the adsorption isotherms for hexosomes and cubosomes after 100 min on the two surfaces. To further explore the adsorption thermodynamics, the isotherms in Figure 5 were fitted, using the Langmuir model. The Langmuir adsorption isotherm can be written as

$$\Gamma = \Gamma_\infty \frac{Kc}{1 + Kc}$$

where Γ_∞ is the plateau-adsorbed amount (mg m^{-2}), c is the particle concentration (mol m^{-3}), and K is the equilibrium adsorption constant. Correlation coefficients for fits of the particle adsorption data to the Langmuir model are in the range 0.96−0.99, supporting the application of the model to these systems. The corresponding Γ_∞ and K values are given in Table 3 along with the free energy of adsorption (ΔG°) calculated from

$$\Delta G^\circ = -RT \ln K$$

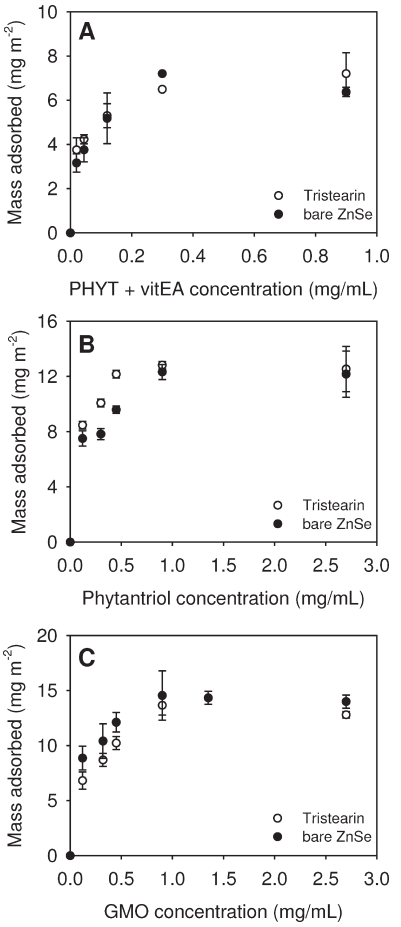

Figure 5. Adsorption isotherms at 100 min for PHYT + VitEA hexosomes (A), PHYT cubosomes (B), and GMO cubosomes (C) on TS-coated and ZnSe surfaces (mean ± SD; n = 3).

Table 3. Langmuir Model Parameters for LC Particle Adsorption at the Surfaces

particle	surface	Γ_∞ (mg m^{-2})	K	ΔG° (kJ mol^{-1})
PHYT + VitEA	ZnSe	7.0	14.4	6.6
hexosome	tristearin	7.0	10.9	5.9
PHYT	ZnSe	13.2	2.1	1.9
cubosome	tristearin	13.3	4.7	3.8
GMO	ZnSe	15.1	3.4	3.0
cubosome	tristearin	14.3	2.2	2.0

where R is the general gas constant (8.314 J K^{-1} mol^{-1}) and T the absolute temperature (298 K).

The adsorption of PHYT + VitEA hexosomes plateaued at a value of approximately 7.0 mg m^{-2} at both ZnSe and TS-coated surfaces (Figure 5A), significantly lower than that of cubosomes. For PHYT cubosomes, the average adsorption plateau values for ZnSe and TS-coated surfaces were 13.2 and 13.3 mg m^{-2}, respectively. GMO cubosomes showed adsorption values comparable to those of PHYT cubosomes; the average adsorption plateau values for ZnSe and TS-coated surfaces were 15.1 and 14.3 mg m^{-2}, respectively (Figure 5C).

The PHYT + VitEA hexosomes have the highest ΔG° values compared to the cubosomes. The differences in the ΔG° values

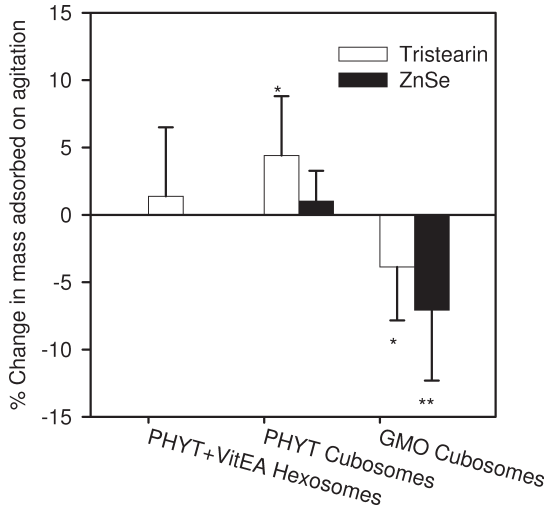

Figure 6. Percent change in the mass of material adsorbed on the ZnSe and TS-coated surfaces after 2 min of agitation (mean ± SD; $n \geq 9$): (*) $P < 0.01$; (**) $P < 0.001$; paired t test of the mass adsorbed before and after agitation.

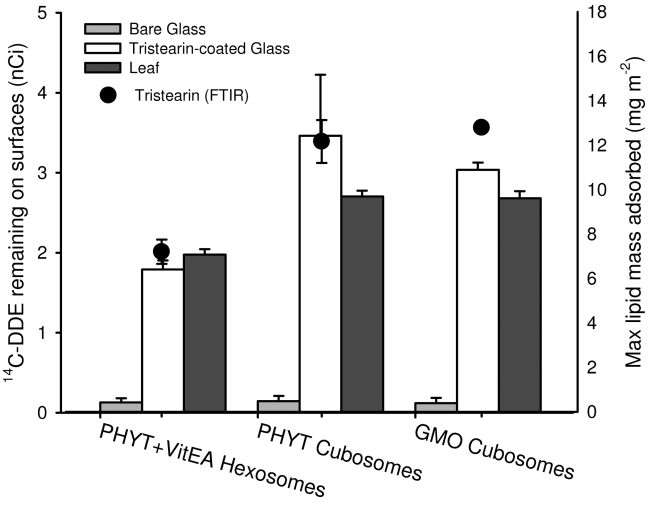

Figure 7. Radioactivity remaining on the surface of TS-coated and uncoated glass coverslips and on *Hebe* leaves, after immersion in different ^{14}C-DDE-loaded LC dispersions for 3 h (bars, mean ± SEM; $n \geq 5$), compared with the maximum mass of LC dispersed systems adsorbed on the tristearin layer after 100 min from the FTIR study (circles, mean ± SD; $n = 3$).

between the ZnSe (6.6 kJ mol^{-1}) and TS-coated (5.9 kJ mol^{-1}) surfaces were within experimental error, suggesting that the type of surface had only a small or no bearing on the overall adsorption isotherms. For GMO cubosomes, again there was no statistically significant difference for $\Delta G°$ values between the ZnSe (3.0 kJ mol^{-1}) and TS-coated (2.0 kJ mol^{-1}) surfaces, suggesting that the surface chemistry only makes a minor contribution to their surface adsorption. In contrast, the PHYT cubosome showed a statistically lower $\Delta G°$ value for adsorption at the ZnSe surface (1.9 kJ mol^{-1}) than at the TS-coated surface (3.8 kJ mol^{-1}), suggesting that the nature of the surface does affect its adsorption.

Effect of Agitation. Figure 6 shows the percent change in the mass of material adsorbed on the bare ZnSe and TS-coated surfaces after 2 min of agitation, as an indication of the relative strength of the surface adhesion of particles. The agitation process caused a significant decrease in the surface mass adsorbed for the GMO cubosome system. In comparison, the agitation process did not cause any significant decrease in the mass adsorbed for PHYT-based cubosomes and hexosomes at either surface. The PHYT cubosome system showed a slight increase in the mass adsorbed on the TS-coated surface, after agitation. This indicates that the GMO cubosome system was more easily displaced from the bare ZnSe and TS-coated surfaces than the PHYT-based systems.

Delivery of Hydrophobic Actives to Surfaces Using LC Particles as Vehicles. Figure 7 shows the DDE (indicated by radioactivity) remaining on the surface of TS-coated and uncoated glass coverslips and on *Hebe* leaves, after immersion in different LC dispersions for 3 h. The trends in adsorption for different particles at the leaf surface were similar to that for TS-coated glass coverslips, indicating the relevance of the TS-coated surface as a model for studying adsorption to foliar surfaces.

There was negligible radioactivity associated with the uncoated glass surfaces after 3 h. This result indicates that the adsorption on the uncoated side of the TS-coated coverslips was negligible (although it was, nevertheless, subtracted from the total for the tristearin experiments).

The DDE retained on the TS-coated surface after immersion in PHYT + VitEA hexosome dispersions was significantly lower than for that PHYT and GMO-based cubosome dispersions. To allow a direct comparison with FTIR data, Figure 7 also shows the maximum mass of material adsorbed for each system on the tristearin layer after 100 min from the FTIR adsorption study. The differences in the relative mass of LC particles adsorbed were in agreement with the relative differences in the amount of radioactivity remaining on the surface of the TS-coated coverslip (r^2 = 0.98). This indicates a relationship between the mass of lipid adsorbed at the surface and the amount of active agent remaining on the surface; i.e., the more LC particles adsorbed, the greater the radioactivity remaining.

DISCUSSION

Correlation between Particle Adsorption and Active Delivery. The primary motivation for this study was to establish the adsorption behavior of lipid-based cubosomes and hexosomes to biorelevant surfaces as an indicator of their potential as agrochemical delivery systems. This study has shown that there is a good correlation between trends in the mass of lipid adsorbed and the DDE remaining on the tristearin and leaf surfaces after incubation with DDE-loaded particles. This confirms that the hydrophobic active was retained within the LC particles during adsorption, and hence the efficiency of the active delivery is dependent on the efficiency of LC particle adsorption at the surfaces. Had the active adsorbed to the surface from a free solution rather than being encapsulated in the particle, we would not expect to see a difference between the different delivery systems, much less a direct correlation with the quantities of lipid adsorbed from the FTIR studies. PHYT-based hexosomes were less efficient as delivery agents to hydrophobic surfaces than the cubosome systems, which has implications for the selection of formulations across a range of applications where the adsorption at surfaces is important in the outcome.

Particle Adsorption Behavior. There are a number of properties of these systems that might be expected to impact particle adsorption, including the size, particle morphology, surface hydrophobicity, role of the stabilizer, and characteristics of the substrate.

Size and Morphology. The different LC particles used in this study were of comparable size and size distribution (Table 1). Therefore, it is unlikely that the particle size has played a significant role in the differences in the adsorption behavior between the LC particles.

The external morphology of cubosomes and hexosomes has been well studied using cryo-transmission electron microscopy (TEM), cryo-field emission scanning electron microscopy (FESEM),[45,46] atomic force microscopy (AFM),[47] and mathematical modeling.[48,49] Cryo-TEM studies have led to the proposition that hexosomes exist as flat hexagonal prisms,[50] which, if adsorption was to occur "face-down" on the surface, could explain the reduced quantity of lipid adsorbed for hexosomes compared to cubosomes. However, cryo-FESEM imaging in three dimensions has indicated that hexosomes may also exhibit a "spinning-top" like structure,[46] in which case it would be expected that the quantity of lipid adsorbed per unit area for monolayer packing would be similar to that of cubosomes.

Cubosome systems often contain a certain percentage of vesicles (Figure 1B,C).[51,52] The concentration of vesicles relative to that of cubosomes varies depending on the sample preparation method.[51] In comparison, hexosome systems are generally found to be absent of vesicles (Figure 1A).[52] Vesicles of size equivalent to that of cubosomes and hexosomes contain significantly less lipid. Therefore, if vesicles within the cubosome system were adsorbed at the surface in place of the cubosomes, one would expect a significantly lower quantity of lipid adsorption to be detected for the cubosome systems compared to the hexosome systems. In this study, both GMO and PHYT cubosomes showed higher lipid adsorption than hexosomes; therefore, vesicle adsorption is unlikely to be a significant factor in the difference between the adsorption of cubosome and hexosomes in this study.

Surface Hydrophobicity and Interaction with Stabilizer. Cubosomes and hexosomes require the presence of a steric stabilizer in order to prevent rapid flocculation, because of insufficient repulsive forces to prevent hydrophobic force-driven aggregation. The amount of stabilizer required, the lipid used to form the LC structures, and the preparation method all impact the colloidal stability in such dispersions. Particles with very strong colloidal stabilization would be reasonably expected to avoid adhesion to hydrophobic surfaces. Hence, the development of these particles for optimal delivery to hydrophobic surfaces requires an understanding, and, if possible, control over the interaction between the stabilizer and the surface of the particle, to solve the apparent paradox of, on the one hand, the practical requirement for colloidal stability and, on the other hand, the achievement of enhanced adhesion to hydrophobic surfaces.

Pluronic F127 is the most commonly used steric stabilizer for stabilization of nonlamellar LC particles because it provides the highest degree of colloidal stability reported to date.[53] However, disposition of the steric stabilizer at the interface of the LC particles with a continuous medium is not yet well understood. It has been hypothesized that the hydrophobic moieties [poly(propylene oxide), PPO] are adsorbed at the outer particle surface, while the hydrophilic moieties [poly(ethylene oxide), PEO] extend into the surrounding bulk water, providing steric stabilization.[11,54] As such, one would expect adsorption of the LC particles to be dictated by the interaction of the PEO chain with the substrate surface. This is supported by the faster rate of adsorption on the more hydrophilic ZnSe surface for all LC systems tested (Table 2). However, if the PEO chain−surface interaction was the dominating factor in adsorption of the LC particles on surfaces, given the similar size distribution between all three particle systems (Table 1), one would expect similar adsorption behavior in the FTIR study. This was not observed in this experiment. Furthermore, the previously suggested model of interaction between F127 and LC particles is based on interactions between simple hydrophobic surfaces and F127.[55] LC particles consist of amphiphilic molecules and water, with nonuniform nodular structure at the interface with bulk water. The surfaces of the LC particles are therefore, unlikely to be represented by simple hydrophobic surfaces. As such, the interaction between F127 and LC particles is likely to be much more complex.

Liposomes consist of amphiphilic molecules (typically phospholipids) dispersed in excess water and, hence, are analogous to cubosomes and hexosomes. It has been proposed that copolymers such as F127 interact with liposomes by insertion and anchoring of the PPO chain into the bilayers, either parallel to the acyl chains of the lipid layers or in a flat configuration, leaving the PEO chains to extend in excess water.[56] Such configurations are likely to affect the bilayer curvature. In the case of GMO cubosomes, the presence of F127 causes a change in the cubic phase from $V_{2(Pn3m)}$ to $V_{2(Im3m)}$, indicating an interaction between the bilayer and F127 similar to that of liposomes.[13] In contrast, the addition of F127 (up to 30% w/w relative to lipid) does not change the internal structure of PHYT cubosomes.[19] As such, we hypothesize that F127 is adsorbed to the particle surface for PHYT cubosomes in a manner similar to that of simple hydrophobic surfaces, with PPO chains adsorbed at the cubosome surface and PEO chains extending into the excess water. Furthermore, we hypothesize that this mode of adsorption is a weaker interaction than that when PPO is intercalated into the bilayer, i.e., that F127 is only loosely adsorbed on the surface of PHYT cubosomes. This, in turn, suggests the likelihood that desorption of F127 from PHYT cubosomes is more likely than that from GMO cubosomes. GMO cubosome dispersions are anecdotally more colloidally stable than PHYT dispersions over time. That is consistent with the idea of the loose association of F127 with the surface of PHYT cubosomes, leading to the increased probability of encounter between hydrophobic surfaces compared to GMO cubosomes, in which a more coherent layer of PEO is likely present at the surface. It is then not surprising that a stronger interaction of PHYT cubosomes was found with the more hydrophobic TS-coated surface reflected in the greater free energy of adsorption than on the bare ZnSe surface (Table 3).

Hence, we propose a model for interaction of these particles in which the strong association of F127 with GMO cubosomes inhibits strong particle adsorption to the surface, whereas desorption of F127 from PHYT particles yields stronger hydrophobic interactions with the surface (Figure 8).

The model is also consistent with the tendency of GMO cubosomes to desorb in the agitation test compared to PHYT cubosomes (Figure 6). The susceptibility of GMO cubosomes to desorb from the surface agrees, at least in part, with the reported interaction of GMO cubosomes with a DOPC bilayer, in which lipid extraction/detergency was reported rather than strong or

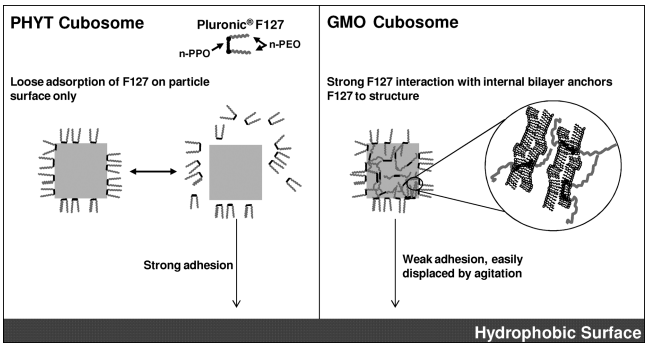

Figure 8. Hypothesized model of the interaction between F127 and GMO or PHYT-based cubosomes and the consequent effect of such an interaction on the cubosome adsorption behavior on hydrophobic surfaces.

irreversible surface adhesion (bearing in mind the substantial difference between a fluid phospholipid bilayer and solid tristearin).[36]

The ability of PHYT cubosomes to withstand agitation has important implications for their practical use in agricultural application where resistance to mechanical displacement can provide rainfastness and an enhanced opportunity for agricultural agent absorption into the leaf structure. There was, in fact, a slight increase in the mass adsorbed for the PHYT cubosome system on the TS-coated surface (after agitation); while the reason for this is unclear, one explanation is that the agitation process removes loosely bound aggregates, exposing fresh substrate for more effective coverage to occur. The agitation experiment was done predominantly to satisfy curiosity on the effect of agitation on adsorbed particles and, as such, the method of agitation is likely to be of little relevance to the actual perturbation experienced by LC particles when applied to the leaf surface in field settings. Nevertheless, the experiment provides serendipitous insight into the particle adsorption behavior and highlights the differences between the behavior of LC particles.

The model for differences in cubosome adsorption is less able to explain the behavior of the hexosomes. The faster rate of adsorption on the more hydrophilic ZnSe surface (Table 2) suggests that F127 does play a significant role in the particle adsorption, similar to the cubosomes. However, the significantly higher adsorption rate (Table 2) and adsorption free energy (Table 3) but lower mass of adsorption compared to the cubosomes suggest that its adsorption is dictated by other factors. The adsorption of the "flat" hexosomes face-down mentioned earlier may, in part, explain the reduced amount of adsorbed lipid. However, the interpretation in terms of the interaction with F127 is more difficult. The VitEA present in the hexosome is believed to largely locate at the triangular interstices between the hexagonally packed water channels, filling the void between PHYT chains that would otherwise occur upon strict uniform packing in the case of PHYT alone.[18] This stabilizes the hexagonal phase to formation at a lower temperature. The major component of the hexosomes is still PHYT; as such, we hypothesize that F127 is loosely bound to the hexosome surface, similar to the PHYT-based cubosomes.

Furthermore, it has been suggested that the interface between the hexagonal phase and excess water can be satisfied through capping of the aqueous channels via nodule formation.[46,57] This requires the lipids, which prefer to form inverse phase structures, to adopt in some regions an unfavorable "normal" geometry. The higher energy state of the hexosomes due to the unfavorable geometry may explain its rapid and high energy of surface adsorption compared to the cubosomes because the surface adsorption process eliminates the nodule formation and hence unfavorable geometry.

Substrate Effects. In the context of this study, we are most interested in the behavior of LC particles at the TS-coated surface; however, some comments comparing the behavior at different surfaces should be made. Changes in the IR spectra for adsorbed GMO cubosomes between the bare ZnSe and TS-coated surfaces (Figure 3) suggest differences in the lipid packing order after adsorption. There was also an equivalent or slightly greater adsorption of lipid for GMO cubosomes at the ZnSe surface that was not apparent for PHYT cubosomes. Vandoolaeghe et al. observed GMO cubosomes on hydrophobic surfaces, with the formation of a thin unimer layer suggestive of structural relaxation at the surface, which may be suggestive of some wetting of the surface by the lipids comprising the particles, leading to a flattening of the adsorbed particles and, in turn, leading to fewer particles per unit area adsorbed at the surface. In contrast, a greater mass of adsorption occurred on a hydrophilic silica surface, as thicker aggregates with minimal structural relaxation.[34,37] Similarly, adsorption at the hydrophilic ZnSe surface in the current study may not allow structural relaxation of the GMO cubosomes on the surface, leading to greater mass adsorbed. The structural relaxation on the surfaces may also explain the lower quantity of hexosomes adsorbed on the surface compared to cubosomes. We hypothesized earlier that the hexosomes showed a greater rate and free energy change of adsorption due to unfavorable geometry present in the system, which is partially relieved upon particle adsorption. Similarly, once the hexosomes are adsorbed at the surface, they may also experience greater structural relaxation and hence greater spread than cubosomes. The greater spread of the hexosomes on the surface then, in turn, leads to fewer particles per unit area than cubosomes.

While the absolute adsorption of particles at the surface is the parameter of direct interest, further studies are planned using quartz crystal microbalance and AFM to better understand the nature of the film formed in terms of thickness and rigidity.

Last, the additional complication of using F127, a relatively hydrophilic stabilizer, is that a proportion is expected to exist as free monomers in the solution, and possibly as micelles. Therefore, there is the potential for adsorption at the substrate from solution. This may also induce a steric barrier, leading to possible complications of the adsorption behavior. However, the same level of F127 was used across the particles in this study with very different results, indicating that if adsorption of F127 occurs to the substrate, it does not dominate the adsorption behavior of particles from the dispersion; otherwise, similar results would have been expected across the different systems. The adsorption of particles indicates that if F127 does adsorb at the surfaces, it is easily displaced by the particles.

CONCLUSIONS

The adsorption behavior of dispersed LC systems on different surfaces was investigated in this study. The internal structure and lipid from which the particles were prepared were found to influence the particle adsorption properties, with the following:

1 Cubosomes showed higher mass but lower rate and free energy change upon adsorption than hexosomes.

2 Cubosomes showed greater localization of the active to the TS-coated surface than hexosomes, indicating a close correlation between LC mass adsorption and active surface localization.
3 GMO cubosomes showed weaker surface adhesion compared to PHYT cubosomes because they were easily displaced from surfaces via agitation.

The strong particle adsorption and adhesion for PHYT cubosomes compared to GMO cubosomes and high localization of the active agent to the surface compared to PHYT-based hexosomes indicate their better candidature as agrochemical delivery systems. These findings highlight the implications of understanding the interfacial behavior of LC systems for application in the delivery of encapsulated agents to surfaces.

AUTHOR INFORMATION

Corresponding Author
*E-mail: ben.boyd@monash.edu.

ACKNOWLEDGMENT

The authors thank the Kerry Bio-Science (Norwich, NY) for donation of Myverol 18-99K. Y.-D.D. thanks Monash University for support in the form of an Australian Postgraduate Award scholarship and a postgraduate publication award scholarship.

REFERENCES

(1) Kaasgaard, T.; Drummond, C. J. *Phys. Chem. Chem. Phys.* **2006**, *8*, 4957–4975.
(2) Wells, D.; Fong, C.; Drummond, C. J. *J. Phys. Chem. B* **2006**, *110*, 5112–5119.
(3) Fong, C.; Weerawardena, A.; Sagnella, S. M.; Mulet, X.; Waddington, L.; Krodkiewska, I.; Drummond, C. J. *Soft Matter* **2010**, *6*, 4727–4741.
(4) Sagnella, S. M.; Conn, C. E.; Krodkiewska, I.; Moghaddam, M.; Drummond, C. J. *J. Phys. Chem. B* **2010**, *114*, 1729–1735.
(5) Chang, C. M.; Bodmeier, R. *J. Pharm. Sci.* **1997**, *86*, 747–752.
(6) Chang, C. M.; Bodmeier, R. *J. Controlled Release* **1997**, *46*, 215–222.
(7) Sadhale, Y.; Shah, J. C. *Int. J. Pharm.* **1999**, *191*, 51–64.
(8) Shah, J. C.; Sadhale, Y.; Chilukuri, D. M. *Adv. Drug Delivery Rev.* **2001**, *47*, 229–250.
(9) Drummond, C. J.; Fong, C. *Curr. Opin. Colloid Interface Sci.* **1999**, *4*, 449–456.
(10) Landh, T. *J. Phys. Chem.* **1994**, *98*, 8453–8467.
(11) Gustafsson, J.; Ljusberg-Wahren, H.; Almgren, M.; Larsson, K. *Langmuir* **1996**, *12*, 4611–4613.
(12) Gustafsson, J.; Ljusberg-Wahren, H.; Almgren, M.; Larsson, K. *Langmuir* **1997**, *13*, 6964–6971.
(13) Nakano, M.; Sugita, A.; Matsuoka, H.; Handa, T. *Langmuir* **2001**, *17*, 3917–3922.
(14) Nakano, M.; Teshigawara, T.; Sugita, A.; Leesajakul, W.; Taniguchi, A.; Kamo, T.; Matsuoka, H.; Handa, T. *Langmuir* **2002**, *18*, 9283–9288.
(15) Borne, J.; Nylander, T.; Khan, A. *Langmuir* **2000**, *16*, 10044–10054.
(16) Borne, J.; Nylander, T.; Khan, A. *Langmuir* **2001**, *17*, 7742–7751.
(17) Abe, S.; Takahashi, H. *J. Appl. Crystallogr.* **2003**, *36*, 515–519.
(18) Dong, Y.-D.; Dong, A. W.; Larson, I.; Rappolt, M.; Amenitsch, H.; Hanley, T.; Boyd, B. J. *Langmuir* **2008**, *24*, 6998–7003.
(19) Dong, Y.-D.; Larson, I.; Hanley, T.; Boyd, B. J. *Langmuir* **2006**, *22*, 9512–9518.
(20) Barauskas, J.; Svedaite, I.; Butkus, E.; Razumas, V.; Larsson, K.; Tiberg, F. *Colloids Surf., B* **2005**, *41*, 49–53.
(21) Spicer, P. T. *Dekker Encycl. Nanosci. Nanotechnol.* **2004**, 881–892.
(22) Fong, C.; Krodkiewska, I.; Wells, D.; Boyd, B. J.; Booth, J.; Bhargava, S.; McDowall, A.; Hartley, P. G. *Aust. J. Chem.* **2005**, *58*, 683–687.
(23) Bender, J.; Ericson, M. B.; Merclin, N.; Iani, V.; Rosen, A.; Engstrom, S.; Moan, J. *J. Controlled Release* **2005**, *106*, 350–360.
(24) Richert, S.; Schrader, A.; Schrader, K. *Int. J. Cosmet. Sci.* **2003**, *25*, 5–13.
(25) Esposito, E.; Cortesi, R.; Drechsler, M.; Paccamiccio, L.; Mariani, P.; Contado, C.; Stellin, E.; Menegatti, E.; Bonina, F.; Puglia, C. *Pharm. Res.* **2005**, *22*, 2163–2173.
(26) Kwon, T.; Lee, H.; Kim, J.; Shin, W.; Park, S.; Kim, J.-C. *Colloid J.* **2010**, *72*, 205–210.
(27) Kwon, T. K.; Kim, J.-C. *J. Dispersion Sci. Technol.* **2010**, *31*, 1004–1009.
(28) Herai, H.; Gratieri, T.; Thomazine, J. A.; Bentley, M. V. L. B.; Lopez, R. F. V. *Int. J. Pharm.* **2007**, *329*, 88–93.
(29) Lopes, L. B.; Collett, J. H.; Bentley, M. V. L. B. *Eur. J. Pharm. Biopharm.* **2005**, *60*, 25–30.
(30) Bender, J.; Simonsson, C.; Smedh, M.; Engström, S.; Ericson, M. B. *J. Controlled Release* **2008**, *129*, 163–169.
(31) Kim, J.-C.; Lee, K. U.; Shin, W. C.; Lee, H. Y.; Kim, J. D.; Kim, Y. C.; Tae, G.; Lee, K. Y.; Lee, S.-J.; Kim, J.-D. *Colloids Surf., B* **2004**, *36*, 161–166.
(32) Kuntsche, J.; Bunjes, H.; Fahr, A.; Pappinen, S.; Rönkkö, S.; Suhonen, M.; Urtti, A. *Int. J. Pharm.* **2008**, *354*, 180–195.
(33) Vandoolaeghe, P.; Barauskas, J.; Johnsson, M.; Tiberg, F.; Nylander, T. *Langmuir* **2009**, *25*, 3999–4008.
(34) Vandoolaeghe, P.; Campbell, R. A.; Rennie, A. R.; Nylander, T. *J. Phys. Chem. C* **2009**, *113*, 4483–4494.
(35) Vandoolaeghe, P.; Rennie, A. R.; Campbell, R. A.; Nylander, T. *Langmuir* **2008**, *25*, 4009–4020.
(36) Vandoolaeghe, P.; Rennie, A. R.; Campbell, R. A.; Thomas, R. K.; Hook, F.; Fragneto, G.; Tiberg, F.; Nylander, T. *Soft Matter* **2008**, *4*, 2267–2277.
(37) Vandoolaeghe, P.; Tiberg, F.; Nylander, T. *Langmuir* **2006**, *22*, 9169–9174.
(38) Er, Y.; Prestidge, C. A.; Fronasiero, D. *Colloids Surf., B* **2004**, *36*, 147–153.
(39) Misiunas, A. T. Z.; Naiura, G.; Razumas, V. *Biologija* **2004**, 26–29.
(40) Nilsson, A.; Holmgren, A.; Lindblom, G. *Chem. Phys. Lipids* **1994**, *69*, 219–227.
(41) Gugliuzza, A.; De Luca, G.; Tocci, E.; De Lorenzo, L.; Drioli, E. *J. Phys. Chem. B* **2007**, *111*, 8868–8878.
(42) Obata, Y.; Utsumi, S.; Watanabe, H.; Suda, M.; Tokudome, Y.; Otsuka, M.; Takayama, K. *Int. J. Pharm.* **2010**, *389*, 18–23.
(43) de Boer, B.; Frank, M. M.; Chabal, Y. J.; Jiang, W.; Garfunkel, E.; Bao, Z. *Langmuir* **2004**, *20*, 1539–1542.
(44) Parikh, A. N.; Allara, D. L.; Azouz, I. B.; Rondelez, F. *J. Phys. Chem.* **1994**, *98*, 7577–7590.
(45) Rizwan, S. B.; Dong, Y.-D.; Boyd, B. J.; Rades, T.; Hook, S. *Micron* **2007**, *38*, 478–485.
(46) Boyd, B. J.; Rizwan, S. B.; Dong, Y.-D.; Hook, S.; Rades, T. *Langmuir* **2007**, *23*, 12461–12464.
(47) Neto, C.; Aloisi, G.; Baglioni, P.; Larsson, K. *J. Phys. Chem. B* **1999**, *103*, 3896–3899.
(48) Andersson, S.; Jacob, M.; Lidin, S.; Larsson, K. *Z. Kristallogr.* **1995**, *210*, 315–318.
(49) Larsson, K. *J. Dispersion Sci. Technol.* **1999**, *20*, 27–34.
(50) Barauskas, J.; Johnsson, M.; Tiberg, F. *Nano Lett.* **2005**, *5*, 1615–1619.
(51) Barauskas, J.; Johnsson, M.; Johnson, F.; Tiberg, F. *Langmuir* **2005**, *21*, 2569–2577.
(52) Sagalowicz, L.; Mezzenga, R.; Leser, M. E. *Curr. Opin. Colloid Interface Sci.* **2006**, *11*, 224–229.
(53) Boyd, B. J.; Dong, Y.-D.; Rades, T. *J. Liposome Res.* **2009**, *19*, 12–28.

(54) Larsson, K. *J. Phys. Chem.* **1989**, *93*, 7304–7314.
(55) Nejadnik, M. R.; Olsson, A. L. J.; Sharma, P. K.; van der Mei, H. C.; Norde, W.; Busscher, H. J. *Langmuir* **2009**, *25*, 6245–6249.
(56) Liang, X.; Mao, G.; Ng, K. Y. S. *J. Colloid Interface Sci.* **2005**, *285*, 360–372.
(57) Rappolt, M.; Hickel, A.; Bringezu, F.; Lohner, K. *Biophys. J.* **2003**, *84*, 3111–3122.
(58) Misiunas, A.; Niaura, G.; Talaikyte, Z.; Eicher-Lorka, O.; Razumas, V. *Spectrochim. Acta, Part A* **2005**, *62*, 945–957.